



Originally published as:

Korte, M., Holme, R. (2010): On the Persistence of Geomagnetic Flux Lobes in Global Field Models. - *Physics of the Earth and Planetary Interiors*, 182, 3-4, 179-186

DOI: [10.1016/j.pepi.2010.08.006](https://doi.org/10.1016/j.pepi.2010.08.006)

# On the Persistence of Geomagnetic Flux Lobes in Global Holocene Field Models

Monika Korte<sup>a</sup>, Richard Holme<sup>b</sup>

<sup>a</sup>*Helmholtz Zentrum Potsdam, Deutsches GeoForschungsZentrum GFZ, Telegrafenberg, 14473 Potsdam, Germany*

<sup>b</sup>*School of Environmental Sciences, University of Liverpool, Liverpool, L69 3GP, UK*

---

## Abstract

To investigate the longevity and robustness of high-latitude flux patches in the geomagnetic field at the core-mantle boundary, we present time-dependent models of the geomagnetic field for the past 7000 years. Our models use the same data set as previously used for time-dependent archaeomagnetic field modelling, but constrained with additional *priori* models from time averages of field models covering the last 150, 400 and 3000 years. We find that the data are consistent with flux patches existing in both north and south hemispheres for the past 7000 years, and that the northern hemisphere patches at least have highly dynamic behaviour. Simple averaging of the historical field may not be appropriate to obtain a characteristic time-averaged model of the field for comparison with other geophysical observables. Our results should inform geodynamo studies of thermal core-mantle coupling, and of possible long-term structure in the geomagnetic field.

*Key words:* Geomagnetism, flux lobes, archaeomagnetic field, time-averaged field, millennial secular variation.

---

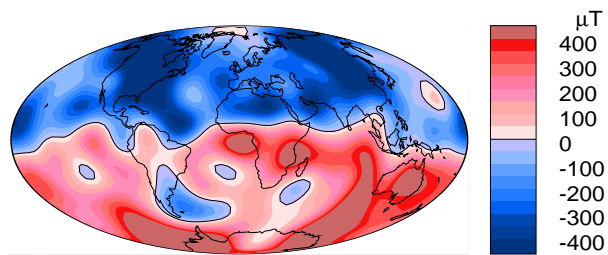
## 1. Introduction

2 Near-surface observations of the geomagnetic field provide a powerful probe of the  
3 dynamics of the top of the Earth's core, and ultimately of the whole geodynamo. Models  
4 of the core surface field have been constructed on a wide range of time scales, from recent,  
5 high-resolution models from satellite data (e.g. Lesur et al., 2008; Olsen et al., 2009),  
6 through time-dependent models of the historical (Jackson et al., 2000) and archaeomagnetic

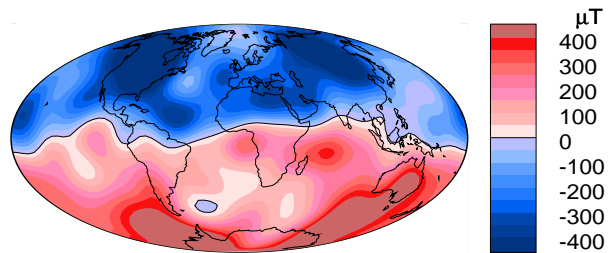
7 field (e.g. Korte and Constable, 2005; Korte et al., 2009), to time-averaged models of the  
8 last 5 Myr paleomagnetic field (e.g., Johnson and Constable, 1995; Kelly and Gubbins,  
9 1997). As the time periods increase, data quality and distribution decrease, leading to  
10 models with lower resolution in both space and time. Nevertheless, there is evidence of  
11 coherent structure in the field on all time scales; such structure is highly significant, and has  
12 been interpreted in terms of mantle control on the geodynamo, through thermal (Bloxham  
13 and Gubbins, 1987) or possibly electromagnetic (Holme, 2000) core-mantle coupling. Two  
14 features of the field have been of particular interest: low secular variation under the Pacific  
15 hemisphere, and stationary flux lobes at high latitudes, possibly in symmetric locations in  
16 the northern and southern hemisphere. It is on the latter patterns that this paper focuses.

17 Figure 1 shows the time-averaged field structure at the core-mantle boundary (CMB)  
18 on four time scales: the historical period from 1840 – 1990 (for which detailed dedicated  
19 observations are available, in particular including absolute magnetic intensity determina-  
20 tions, and time-evolution of the field from magnetic observatories), the longer historical  
21 period from 1590 – 1990 (prior to 1840 dominated by data from ship’s logs (Jonkers et al.,  
22 2003)), the archaeomagnetic field for the past 3000 years (including many sedimentary  
23 records), and for the past 7000 years. Comparison of the averages shows the expected re-  
24 duction in resolution with averaging time, particularly in the southern hemisphere. All the  
25 averaged global models predict the existence of two or three lobes of strongest magnetic  
26 flux in the Northern hemisphere (Bloxham et al., 1989), with similar features observed  
27 in longer term time-averaged global models based on paleomagnetic data from the past  
28 5 million years (Johnson and Constable, 1995; Kelly and Gubbins, 1997). However, the  
29 southern hemisphere flux patches, clear in recent historical and satellite models, are not  
30 seen in the older models.

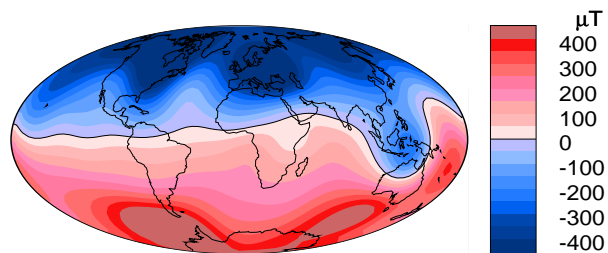
31 It is difficult to decide how much field structure we can expect to resolve with archaeo-  
32 and paleomagnetic data, where data and dating uncertainties are high and often not well-  
33 understood. Simply truncating the spherical harmonic expansion avoids any small-scale  
34 structure, but may map higher degree energy into the lower degree model coefficients. In-  
35 stead, we seek regularised models: models that both fit the data, and also minimise some



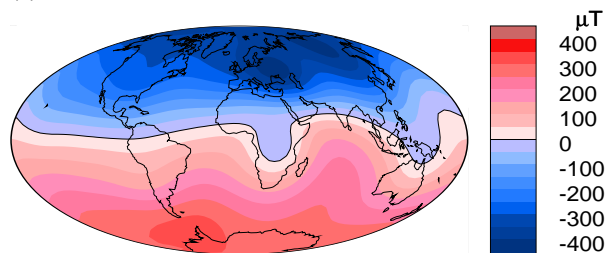
(a) gufm1 Br 1840 AD - 1950 AD



(b) gufm1 Br 1590 AD - 1990 AD



(c) CALS3k.3 Br 1000 BC - 1990 AD



(d) CALS7K.2 Br 5000 BC - 1950 AD

Figure 1: Time averaged radial field component at the core-mantle boundary of the three a priori models and CALS7K.2. (a) and (b) are 150 and 400 year averages, respectively, of *gufm1* by Jackson et al. (2000), (c) and (d) are the overall time averages of CALS3k.3 (Korte et al., 2009) and CALS7K.2 (Korte and Constable, 2005), respectively. Northern hemisphere flux patches are seen at high latitudes under North America and Siberia, and in the more recent models approximately symmetric southern counterparts are seen south of South America and Australia.

36 physical quantity, such as a bound on the electrical dissipation in the dynamo (Gubbins,  
37 1975), the mean square field strength over the CMB, or its time variability. Such assump-  
38 tions bias the solution for the magnetic field towards the minimum magnitude capable of  
39 explaining the observations, and therefore provide a lower bound for the true field strength  
40 or complexity. Formally (in a Bayesian sense) we are seeking a model which fits the data,  
41 subject to an *a priori* model of zero magnitude – that there is no field! This assumption  
42 is clearly not reasonable: the Holocene data clearly indicate the existence of a persistent  
43 field. More specifically, if a time-dependent field model of the archaeomagnetic field sug-  
44 gests episodic flux patches in the north, and none at all in the south, is this because the  
45 data demonstrate that the flux patches are not there at some times, or because the model  
46 is biased towards low magnitudes, and with limited data, the flux patches are eliminated  
47 to reduce the field strength, even (possibly) at the cost of worsened fit to data?

48 To investigate this issue, we seek models of the field which minimise the deviation of  
49 the time-dependent model from a time-averaged model of the field from more recent times,  
50 in which the flux patches are seen clearly. Philosophically, an *a priori* model of a field like  
51 that of the present day seems no more unreasonable than a zero prior, which we know to be  
52 false. By doing this, we investigate whether it is the data or the regularising assumptions  
53 which lead to episodic or missing flux patches. If the models we generate include the flux  
54 patches, then we can argue that there is insufficient evidence to reject the patches being  
55 consistent features in the field; if the patches move around, are episodic or absent, then  
56 we may reject this hypothesis, and make stronger statements about the behaviour of the  
57 centennial and millennial structure of the geomagnetic field.

## 58 **2. Data and a priori models**

59 The data set is the one used to generate CALS7K.2 (Korte and Constable, 2005), which  
60 is readily available from the EarthRef Digital Archive (<http://www.earthref.org>) (Korte  
61 et al., 2005). It consists of directional data from archaeomagnetic studies and lake sediment  
62 records, and intensity data determined from archaeological artefacts and lavas. We realize  
63 that additional data have been published meanwhile, but in order to allow for a comparison

64 to the CALS7K.2 model we retained that data compilation for this study. An iterative  
65 data rejection scheme was used in devising CALS7K.2, and we consider only the final data  
66 set of 27067 values. All data which could not be fit within two average standard deviations  
67 by a first model had been rejected in this dataset (see Korte and Constable, 2005).

68 The choice of the prior model is not straightforward. It is not clear over how long  
69 a time interval the field has to be averaged in order to minimise rapidly varying small-  
70 scale structure to represent properly only persistent larger-scale features. Average over too  
71 short a time period, and rapidly varying features are mapped into the stationary mean  
72 model; over too long a period and we lose structure due to inadequate data distribution  
73 or quality. In order not to make unnecessary assumptions about amount and position of  
74 persistent structure we consider three *a priori* models based on data and without additional  
75 filtering: *gufm1* (Jackson et al., 2000) averaged over the time intervals 1840 to 1990 and  
76 1590 to 1990, and the time-average of the recently published 3kyr model CALS3k.3 (Korte  
77 et al., 2009). All of these averaged models clearly show two pairs of flux lobes, which  
78 are approximately hemispherically symmetric. As testing the compatibility of southern  
79 hemisphere flux lobes with the 7kyr data set is one of our main motivations, we did not  
80 include any longer-term averaged models, which do not show a similarly clear pattern.  
81 The motivation for considering *gufm1* time averages over both 150 and the full 400 years  
82 is twofold: First, 150 years is of the order of the temporal resolution of CALS7K.2 (Korte  
83 and Constable, 2008). Second, the spatial resolution of this model clearly increases with  
84 time as the number and quality of available data increases. In particular, 1840 dates the  
85 establishment of geomagnetic observatories, and also start of widespread measurement of  
86 absolute intensity. The 150 year average is consequently of higher resolution, containing  
87 more smaller scale structure; however, some of this may be present because of insufficient  
88 averaging (Fig. 1a and b). The intensity of the model prior to 1840 is unconstrained by  
89 data (defined only by a backwards-extrapolation of the dipole strength, cite[jackson00]);  
90 this is assumed to be sufficiently close to the real behaviour not to overly bias the average  
91 model structure. The *gufm1* model is calculated to spherical harmonic degree and order 14;  
92 we simply truncated the time-average at degree and order 10 to match the expansion limit

93 of our new models, which seems justified by the fact that with reasonable regularization  
94 all the new models show less power than their priors in spherical harmonic degrees of eight  
95 and higher.

96 The CALS3k.3 model is based on an updated archaeomagnetic and sediment dataset  
97 (Donadini et al., 2009) and spans the time 1000 BC to 1990 AD. Both spatial and temporal  
98 resolution are somewhat higher than for CALS7K.2. The time average (Fig. 1c) contains  
99 significantly less structure than the historical averages, but does show clear flux lobes in  
100 both the northern and southern hemispheres similar to those seen in the *gufm1* averages.

### 101 **3. Four new models**

102 The modelling method is basically the same as used for the *gufm1* (Jackson et al., 2000)  
103 and CALS7K.2 (Korte and Constable, 2005) models and is described in detail there. The  
104 basis functions for the inversion are spherical harmonic functions in space with individual  
105 coefficients expanded in cubic B-splines in time to provide a continuous description (Blox-  
106 ham and Jackson, 1992). Maximum spatial and temporal resolution provided by the basis  
107 functions are higher than the actual resolution considered feasible from the data with their  
108 uncertainties and inhomogeneous global distribution. Regularisations in both time and  
109 space are applied in order to find models with minimum structure required by the data.  
110 Many different models may be appropriate solutions to the inverse problem, ranging from  
111 very smooth models with large misfit to the data to complex models fitting the data closely.  
112 The regularisation parameters (the damping parameters or Lagrange multipliers controlling  
113 the relative penalty assigned to data misfit and model complexity) for the preferred model  
114 are commonly found either from the “knee” of a curve trading off misfit against roughness,  
115 or by fitting the data to the tolerance given by the uncertainty estimates of the data. For  
116 long-term magnetic field models comparisons of resulting time-averaged main field and sec-  
117 ular variation geomagnetic power spectra to models constructed with historical data also  
118 seem suitable criteria, as higher average spatial or temporal complexity, i.e. higher power  
119 in spherical degrees with the exception of 1 and perhaps 2 and 3, is extremely unlikely and  
120 certainly not resolvable with the presently available amount and quality of Holocene data

121 (Korte and Constable, 2008). The chosen regularisation norms result in a damping of power  
 122 in main field and secular variation that increases for higher SH degrees, so that small scale  
 123 / short term structure are efficiently suppressed if the applied regularisation factors result  
 124 in comparable spectral values for the low degrees (Korte et al., 2009).

125 In this study, however, we do not seek an absolute minimum structure model, but the  
 126 minimum deviation from a given average field structure required by the data. We replace  
 127 the constraint of minimising a bound on Ohmic dissipation necessary in the dynamo to  
 128 generate the observed field (Gubbins, 1975), which was used as spatial regularisation for  
 129 both *gufm1* and CALS7K.2, with minimising the radial field deviation at the CMB from  
 130 an *a priori* model, i.e. the quantity

$$S(\mathbf{m}_0) = \int_{CMB} (B_r - B_r(\mathbf{m}_0))^2 d\Omega, \quad (1)$$

131 where  $B_r$  is the radial field of the new model and  $B_r(\mathbf{m}_0)$  that of the *a priori* model  $\mathbf{m}_0$ .  
 132 The integration is performed over solid angle  $d\Omega$  at the core surface, averaged over the  
 133 time period of the model. This condition is easily expressed as a quadratic norm of the  
 134 geomagnetic Gauss coefficients; we minimise

$$\sum_{l=1}^{l_{\max}} \frac{(l+1)^2}{2l+1} \left(\frac{a}{c}\right)^{2l+4} \sum_{m=1}^l [(g_l^m - g_l^m(\mathbf{m}_0))^2 + (h_l^m - h_l^m(\mathbf{m}_0))^2] \quad (2)$$

135 where  $a$  is the radius of the Earth,  $c$  the radius of the CMB,  $\{g_l^m, h_l^m\}$  are the geomagnetic  
 136 Gauss coefficients of spherical harmonic degree  $l$  and order  $m$ , and  $\{g_l^m(\mathbf{m}_0), h_l^m(\mathbf{m}_0)\}$  the  
 137 coefficients of the *a priori* model.

138 Studies of virtual axial dipole moment (McElhinny and Senanayake, 1982; Yang et al.,  
 139 2000) and the previous millennial scale models indicate that the dipole moment has varied  
 140 significantly over the past 7 kyrs. The dipole is the strongest field contribution; we were  
 141 concerned that taking it into account in investigating the required deviation might have  
 142 a dominating influence. Therefore, we also tested models where either the axial dipole  
 143 coefficient, or all three dipole coefficients were not influenced by the spatial regularisation.  
 144 We found that with our criteria for the preferred amount of regularization the differences



145 between these three types of model were small. Nevertheless we retained only the models  
 146 where the dipole was not included in the spatial regularization in the following comparison.

147 The final modelling procedure minimises the functional

$$\text{RMS}^2 + \lambda_S S(\mathbf{m}_0) + \lambda_T T \quad (3)$$

148 with spatial and temporal damping factors (Lagrange multipliers)  $\lambda_S$  and  $\lambda_T$  respectively.

149 The normalised root mean square misfit (RMS) between model predictions  $\hat{x}_i$  and data  $x_i$   
 150 is defined as

$$\text{RMS} = \sqrt{\frac{1}{N} \sum_{i=1}^N \left( \frac{x_i - \hat{x}_i}{\sigma_i} \right)^2}, \quad (4)$$

151 with uncertainty estimates  $\sigma_i$  and  $N$  the number of data. The spatial norm compared with  
 152 the *a priori* model  $\mathbf{m}_0$  is defined in equation (1), and the temporal norm (like the spatial  
 153 norm, averaged over the modelling period) is defined

$$T = \int \left( \frac{\partial^2 B_r}{\partial t^2} \right)^2 d\Omega. \quad (5)$$

154 ( $t$  is time) which can be calculated using a quadratic norm of the form of equation (2).

155 In the end we calculated four new models, summarized in `tabletab:models`. For com-  
 156 parability, we first reconstructed a model M0 similar to CALS7K.2 with zero prior model,  
 157 but regularising by minimising the mean square radial field at the CMB instead of Ohmic  
 158 dissipation norm, and also excluding the dipole coefficients from the regularization. We  
 159 chose the damping factors such that the resulting model shows similar main field and sec-  
 160 ular variation spectra to CALS7K.2 and has a comparable data misfit – the values are  
 161  $\lambda_S = 5 \times 10^{-11}$  and  $\lambda_T = 10^2$ . Three further models were constructed with the same  
 162 damping parameters; the only difference being the *a priori* model. The averaged 150 and  
 163 400 year *gufm1* were used respectively for models M150 and M400. CALS3k.3 was the  
 164 prior model for M3k.

## 165 4. Results

166 As a first step to comparing our models, Figure 2 shows the main field and secular  
 167 variation spectra of the time averages of the four investigated models at the CMB together

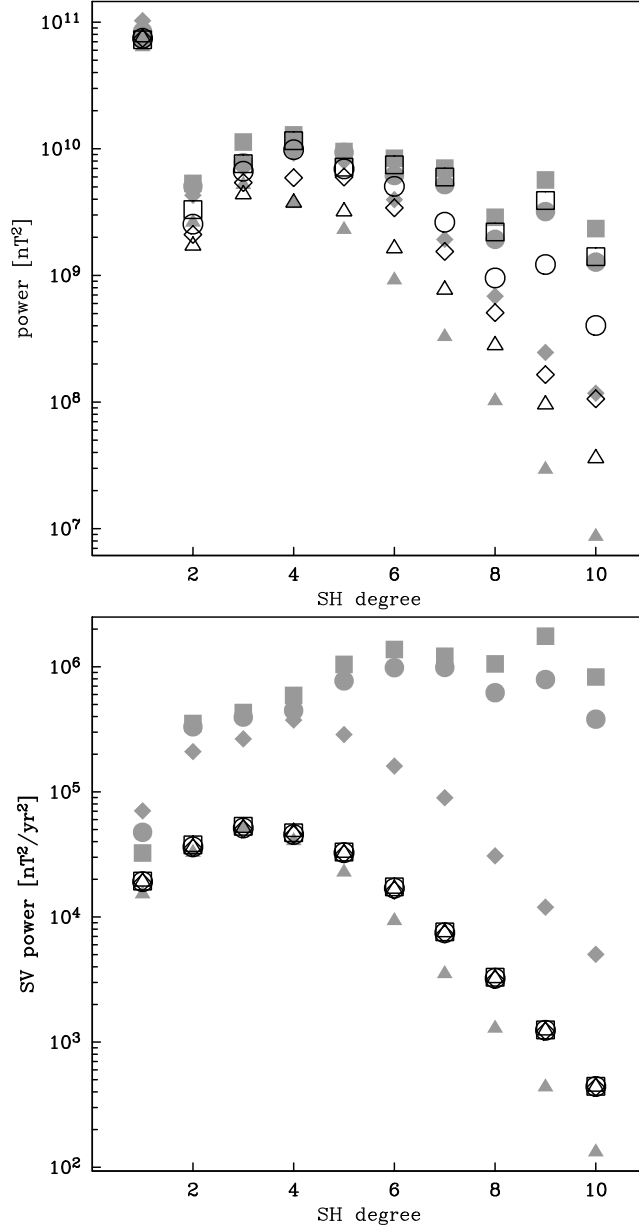


Figure 2: Time averaged main field (top) and secular variation (bottom) geomagnetic power spectra at the core-mantle boundary for models M0 (open triangles), M150 (open squares), M400 (open circles), M3k (open diamonds) and time averaged *gufm1* for 1840 to 1990 (gray squares), 1590 to 1990 (gray circles), CALS3k.3 (gray diamonds) and CALS7K.2 for 5000 BC to 1950 AD (gray triangles).

Table 1: The four new models and their priors.

Model	Prior
M0	0
M150	<i>gumf1</i> averaged from 1840 to 1990
M400	<i>gufm1</i> averaged from 1590 to 1990
M3k	CALS3k.3 averaged over 3kyr

168 with the spectra of the *a priori* models and the CALS7K.2 spectra. By plotting these  
 169 spectra at the CMB we emphasize the differences in higher degrees. The secular variation  
 170 spectra of the four new models look nearly identical, which is not surprising due to the  
 171 common temporal damping applied independently from the spatial damping. The time-  
 172 averaged spectra of the new models clearly resemble those of their respective *a priori*  
 173 models, except in the case of M0 which was designed to be similar to CALS7K.2. The  
 174 increasing deviation with spherical harmonic degree above degree  $l = 5$  between M0 and  
 175 CALS7K.2 is due to the different regularisation applied.

176 We next consider global diagnostics averaged over the whole 7 kyr time interval. We  
 177 calculate the RMS misfit (equation 4), departure from *a priori* model  $S(\mathbf{m}_0)$  (equation 1)  
 178 and temporal norm  $T$  (equation 5). We also consider the overall spatial structure  $S(0)$

$$S(0) = \int_{CMB} B_r^2 d\Omega. \quad (6)$$

179 For M0, with the zero *a priori* model, we obviously have  $S(\mathbf{m}_0) = S(0)$ . These diagnostics  
 180 are given in Table 2. (Note that although the dipole terms are excluded from the damping,  
 181 all of the norm calculations include the dipole components to give quantities that have di-  
 182 rect physical meaning.) The dependence of overall model complexity on the *a priori* model  
 183 is quantified by the values of  $S(0)$ , characterising the overall average model complexity;  
 184 this measure is higher by 29% for M150 than for M0. All data included in the investigated  
 185 dataset for the time interval 1000 BC to 1950 AD form a subset of the data used in the  
 186 construction of CALS3k.3, the *a priori* model for M3k. This will inevitably give a bias in  
 187 our results; the time-averaged CALS3K model is bound to be a good fit to the CALS7K

Table 2: Rms misfit and spatial and temporal complexity of new models

Model	rms	T (nT <sup>2</sup> yr <sup>-4</sup> )	S(0) (nT <sup>2</sup> )	S( <b>m</b> <sub>0</sub> ) (nT <sup>2</sup> )
Time interval 5000 BC to 1950 AD:				
M0	0.989	10.69	$5.9 \times 10^{10}$	$5.9 \times 10^{10}$
M150	0.997	10.85	$7.6 \times 10^{10}$	$2.0 \times 10^{10}$
M400	0.990	10.63	$7.0 \times 10^{10}$	$1.6 \times 10^{10}$
M3k	0.984	10.53	$6.3 \times 10^{10}$	$1.2 \times 10^{10}$
Time interval 5000 BC to 1000 BC:				
M0	0.968	7.87	$4.8 \times 10^{10}$	$4.8 \times 10^{10}$
M150	0.975	7.94	$6.6 \times 10^{10}$	$3.0 \times 10^{10}$
M400	0.961	7.62	$6.0 \times 10^{10}$	$2.3 \times 10^{10}$
M3k	0.956	7.49	$5.3 \times 10^{10}$	$1.6 \times 10^{10}$

188 data set for the period after 1000 BC. To accommodate this bias, we calculate two sets  
189 of diagnostics in table 2, first for the whole 7000 years, and secondly separately for the  
190 time interval 5000 BC to 1000 BC, which is not considered in any of the a priori models.  
191 This second set of diagnostics should eliminate (or at least limit) the bias from considering  
192 common data sets. With so many diagnostics of the models presented, it could be ex-  
193 tremely difficult to determine which prior model is most compatible with the observations;  
194 however, fortunately, the results obtained allow a clear ranking of the models. Comparing  
195 the three models with time-averaged *a priori* model, all four diagnostics (misfit, temporal  
196 norm, absolute spatial norm and departure from *a priori* model) are largest for M150,  
197 intermediate for M400, and smallest for M3k; this ordering applies both for the full time  
198 interval and also for the first 4000 years. Comparing with M0, the model with a zero  
199 prior (the standard damping), all the other models have more spatial power (as would be  
200 expected). Comparing misfit and temporal norm, the M150 model performs less well than  
201 M0, the M400 marginally better, and the M3k substantially better.

202 In conclusion, the data can be fit better by a model requiring less temporal variability if  
203 a suitable *a priori* model is used. Among the a priori models tested the averaged CALS3k.3

204 turns out to be the most suitable, with relatively little deviation required, yet giving the  
205 best fit to the data and least required temporal variation. The data are least compatible  
206 with *gufm1* averaged only over the most recent 150 years.

207 A more detailed analysis of the behaviour of the solution norms as a function of time  
208 is provided in Fig. 3, which plots the mean square radial field, the mean square departure  
209 of the field from the *a priori* model, and the temporal norm as a function of time. The  
210 profiles for the different *a priori* models are generally similar, especially for the temporal  
211 complexity  $T$ . The absolute amount of complexity,  $S(0)$ , shows nearly identical relative  
212 variations with time. The relative deviation from the three non-zero *a priori* models also  
213 is similar, with maximum values around 4000 BC for all, and again between 0 and 1000  
214 AD for the two *gufm1* *a priori* models.

215 The average spatial structure of the models is shown by plots of their mean radial field  
216 at the CMB (Fig. 4). The averages of the different models show clear similarities in large-  
217 scale features, while reflecting the amount of complexity of the *a priori* model (for example,  
218 the small near-equatorial flux patches in M150 are clearly a result of insufficient time-  
219 averaging of the *a priori* model in this region). The available data are clearly compatible  
220 with two southern hemisphere flux lobes which are persistent enough to show up in the  
221 time-averaged model. In all four models, there are three (rather than two) flux lobes  
222 present in the northern hemisphere, despite the prior model for M150 and M400 requiring  
223 only the two lobes seen in today's field. We may therefore be confident that the Holocene  
224 data do require a third northern flux lobe under Europe. A similar flux lobe pattern could  
225 also exist in the southern hemisphere, but none of the prior models show this feature,  
226 and there are insufficient data to constrain this question. Note, however, that even recent  
227 high-resolution field models for one epoch, like e.g. the IGRF for 2005 (Macmillan and  
228 Maus, 2005), show a somewhat similar third flux lobe if truncated at spherical harmonic  
229 degree 5 or 6 (with counterpart in the southern hemisphere). This apparent third flux lobe  
230 therefore might be a manifestation of unresolved but non-averaging smaller scale structure.  
231 Another common feature of all models is an area of positive radial field in the north-western  
232 Pacific, although its detailed form and strength is affected by the different prior models.

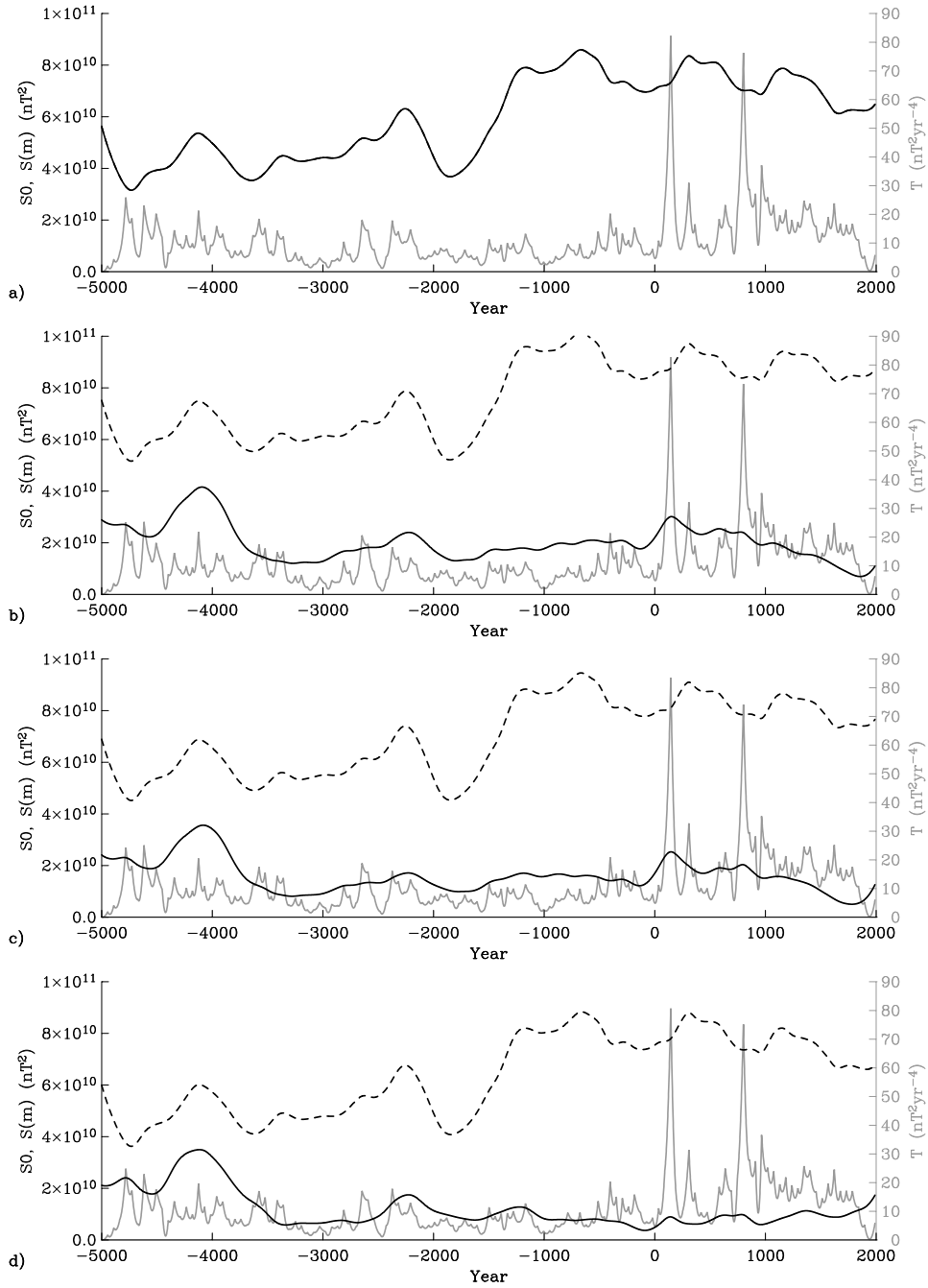
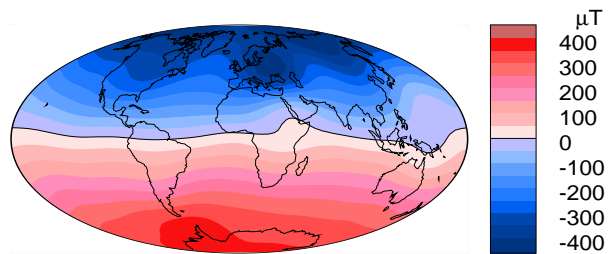
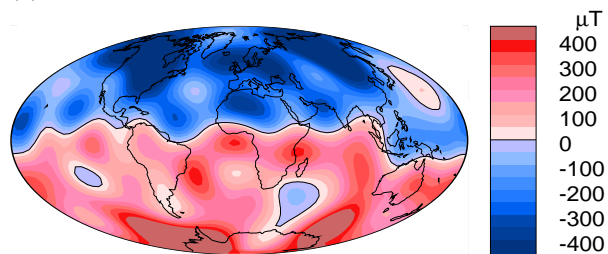


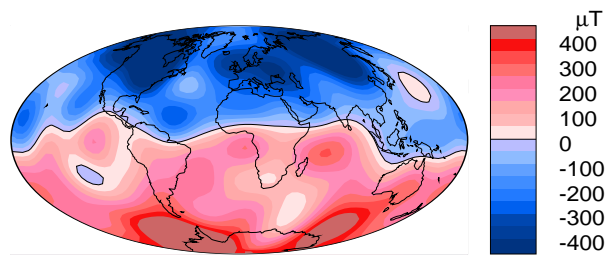
Figure 3: Spatial and temporal complexity as measured by  $S(\mathbf{m}_0)$  (black solid line),  $S(0)$  (dashed line) and  $T$  (gray) for models a) M0, b) M150, c) M400, d) M3k. The solid and dashed lines are by definition identical for M0.



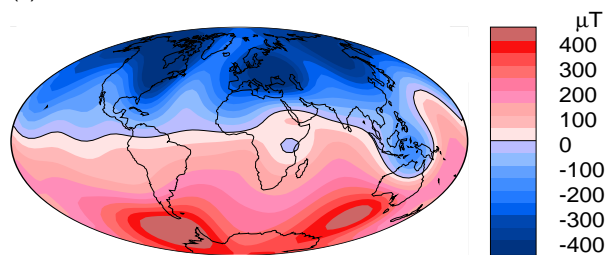
(a) M0 Br 5000 BC - 1950 AD



(b) M150 Br 5000 BC - 1950 AD



(c) M400 Br 5000 BC - 1950 AD



(d) M3k Br 5000 BC - 1950 AD

Figure 4: Time averaged radial field component at the core-mantle boundary of the four new models.

233 This feature has also been seen in previous models (see, for example, the snapshot models  
234 of Constable et al. (2000)), and shows up clearly in longer time-period palaeomagnetic  
235 models (for example, Johnson and Constable, 1997).

236 Animations of the evolution radial field are provided in Fig. 5 (electronic version or  
237 supplemental material) with the present position of flux lobes outlined by the  $\pm 400 \mu\text{T}$   
238 isolines of the 400 yr time-averaged *gufm1* model. These animations show substantial  
239 variability of the flux concentrations on multi-centennial time-scales in all four models,  
240 confirming that they are in fact required by the data and with only minor influence from  
241 the choice of *a priori* model. Despite a large amount of movement and/or decrease and  
242 increase of flux, the flux concentration is rather high most of the time in the area of the  
243 present North American flux lobe, with only two time intervals of significantly weaker flux  
244 spanning about 500 years around 1950 BC and 650 AD. Similarly, the flux concentration  
245 remains high in the area of the present Siberian flux lobe except for 200 to 600 year intervals  
246 around 3450 BC, 1800 BC and 100 BC. Significantly stronger flux than present, however,  
247 appears in the European region for 2 to 5 centuries around 5000 BC, 4500 BC, 2500 BC,  
248 1500 BC, 250 BC and 800 AD. Flux variations are weaker in the southern hemisphere,  
249 likely as a consequence of the sparsity of southern hemisphere data.

## 250 5. Discussion

251 Our primary result is clear and perhaps unsurprising: southern hemisphere flux patches  
252 are consistent with the available data. There is no evidence requiring that they are less  
253 persistent than their northern hemisphere counterparts. However, some interesting further  
254 results emerge from more detailed comparisons. Constraining the model about the 150 year  
255 time average is apparently less appropriate than applying no constraint at all. This suggests  
256 that, although tempting because of the much higher quality data for this period, using this  
257 time average as a proxy for long-term field behaviour is not appropriate. Why might this  
258 be? One possibility is that the averaging time is insufficient to average out small scale  
259 motions (for example, the propagation of flux patches along the equator (Jackson, 2003)),  
260 leaving small scale features to be fit that are not persistent on longer time scales. Another



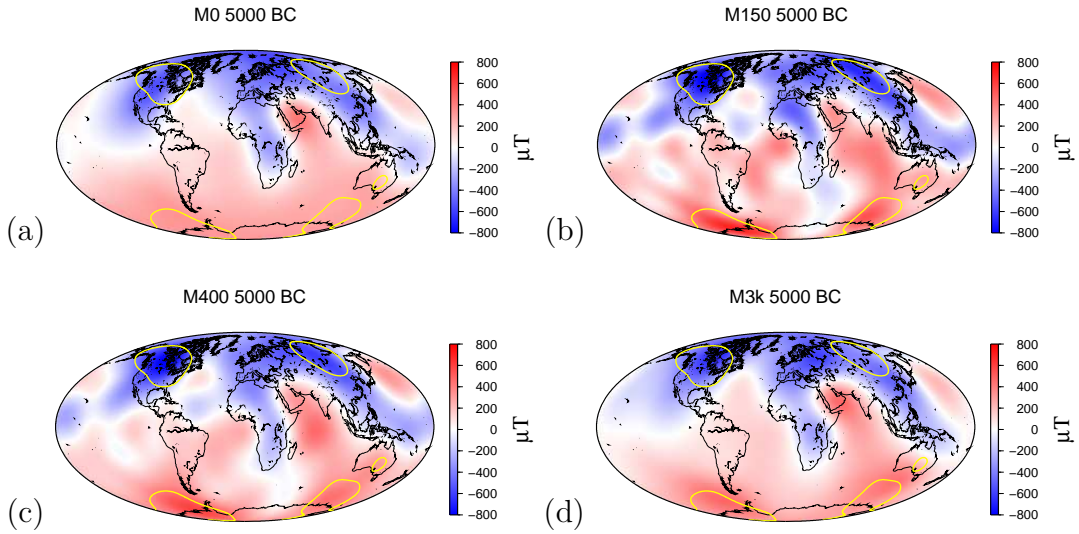


Figure 5: Animations (electronic version or supplemental material) of the radial magnetic field evolution of models (a) M0, (b) M150, (c) M400 and (d) M3k at the CMB. Yellow lines indicate the  $\pm 400 \mu\text{T}$  contour lines of the 400 yr time averaged *gufm1* model.

261 important effect is likely to be the appearance after 1840 of the southern hemisphere  
 262 reversed flux patch, associated by Gubbins (1987) with the current rapid decay of the  
 263 axial dipole field. A third effect is that the particularly strong flux lobes from the *a priori*  
 264 model for M150 act to preclude the variability in the position of the northern hemisphere  
 265 flux lobes; from examination of the movie, there is certainly evidence that the prior model  
 266 is having a strong influence on the position and longevity of these features compared  
 267 with the other three models. Any or all of these explanations suggest that if we wish  
 268 to correlate geomagnetic field morphology with other geophysical observables (e.g. geoid,  
 269 seismic tomography), then the recent historical field or even high-resolution models of the  
 270 current field from satellite data may be less appropriate than the longer term averages.

271 It is interesting to note that all three models using *a priori* field averages for regular-  
 272 ization clearly indicate the existence of three large northern hemisphere areas of high flux  
 273 concentration on average (Fig. 4), while the historical field averages (and present field)  
 274 mainly show two (Fig. 1). The highly dynamic evolution of the flux pattern over time,  
 275 however, makes it difficult to clearly distinguish between lateral movements of flux patches  
 276 and growth and decay of regional flux concentrations. Interestingly, a strong appearance of

277 all three flux patches simultaneously is rare. Their movement with time is also significant,  
278 because the prior models (M150 in particular) favour restraining them to a single location;  
279 that they are nonetheless variable in their positions suggests that this is a true feature  
280 of the field required by the data. Nevertheless, the dynamic nature of the flux patches  
281 has important implications for numerical dynamo studies of thermal core-mantle exam-  
282 ple. For example, in their dynamo calculations, Willis et al. (2007) have located a region  
283 of parameter space (admittedly far from Earth-like) in which a numerical dynamo code  
284 yields flux lobe patterns similar to field observed for the present day. These patches are  
285 dynamic, moving around and occasionally dividing, but none the less, apparently less dy-  
286 namic than the behaviour implied by the observations and our modelling here. Additional  
287 study (Davies et al., 2008) has located a parameter regime with evidence of the three-fold  
288 symmetry we observe in our models; our models suggest that an evaluation of the tran-  
289 sition between these two regimes would be of great interest. No corresponding southern  
290 hemisphere counterpart for the third flux lobe centered under Europe appears. This is  
291 not surprising as our a priori models do not encourage this, and the southern hemisphere  
292 data are sparse. However, the three models do suggest a region of weak to reversed flux  
293 under southern Africa and surrounding areas, roughly the same region as the present day  
294 Southern Atlantic Anomaly (Gubbins and Bloxham, 1985). Together with the appearance  
295 of a strong reverse flux patch around Southern Africa in the first two millennia of the mod-  
296 els, this might be interpreted as a preferred area for the recurrence of significant reverse  
297 flux and consequently minimum field strength. However, this southern hemisphere feature  
298 results from the strong inclination variation seen in one African sediment record between  
299 4000 and 5000 BC (Lake Victoria by Mothersill (1996)). The reverse flux area south of  
300 the equator seen in the averages in Fig. 4 disappears if this specific sediment record is  
301 omitted from the modelling. To our knowledge there are to date no data to the south of  
302 that location between Argentina and Australia to support or contradict the strong effect  
303 of these data on the model. Until such data are available this model feature should be  
304 regarded with caution.

## 305 **6. Conclusions**

306 We have investigated persistent structure in the time-averaged geomagnetic field on  
307 time-scales from centuries to millennia. The deviation from different time-averaged field  
308 models has been used as regularization constraint for spatial structure in modelling the  
309 7kyr dataset which had previously been used for the CALS7K.2 model. Comparisons of  
310 misfit and temporal variability resulting with fixed modelling parameters show that the  
311 data are less compatible with field averages of the past 150 or 400 years than with a 3kyr  
312 average. This indicates that small-scale structure present in field averages of a few centuries  
313 is not persistent on longer time-scales. The smallest misfit between data and model is  
314 obtained, however, if a 3kyr average instead of a zero assumption is used as smoothing  
315 constraint. Distinct northern and southern hemisphere flux lobes are clearly compatible  
316 with the available data spanning the past 7kyrs. Note, however, that persistence in time  
317 averages of the field does not exclude significant temporal variations on shorter intervals;  
318 indeed, from the detailed temporal behaviour there is evidence for considerable variability  
319 in these features.

320 However, clever modelling can take us only so far. While we have demonstrated that  
321 currently available data do not preclude southern hemisphere flux patches, only by ex-  
322 panding the data base for this region can we truly determine the long-term morphology  
323 and variability of the southern hemisphere magnetic field.

## 324 **Acknowledgements**

325 We thank two anonymous reviewers who provided very constructive comments that  
326 improved the manuscript. Funding for RH and the collaboration which produced this  
327 research was provided by NERC grant NER/O/S/2003/00675. The project was completed  
328 with support of a DAAD travel grant.

## 329 **References**

330 Bloxham, J., Gubbins, D., 1987. Thermal core-mantle interactions. *Nature* 325, 511–513.

- 331 Bloxham, J., Gubbins, D., Jackson, A., 1989. Geomagnetic secular variation. *Philos. Trans.*  
332 *R. Soc. London Ser. A* 92, 415–502.
- 333 Bloxham, J., Jackson, A., 1992. Time-dependent mapping of the magnetic field at the  
334 core-mantle boundary. *J. Geophys. Res.* 97, 19,537–19,563.
- 335 Constable, C. G., Johnson, C. L., Lund, S. P., 2000. Global geomagnetic field models for  
336 the past 3000 years: transient or permanent flux lobes? *Phil. Trans. R. Soc. Lond. A*  
337 358, 991–1008.
- 338 Davies, C. J., Gubbins, D., Willis, A. P., Jimack, P. K., 2008. Time-averaged paleomagnetic  
339 field and secular variation: Predictions from dynamo solutions based on lower mantle  
340 seismic tomography. *Phys. Earth Planet. Int.* 169, 194–203.
- 341 Donadini, F., Korte, M., Constable, C., 2009. Geomagnetic field for 0-3ka: 1.  
342 new data sets for global modeling. *Geochem. Geophys. Geosys.* 10, Q06007,  
343 doi:10.1029/2008GC002295.
- 344 Gubbins, D., 1975. Can the Earth's magnetic field be sustained by core oscillations? *Geo-*  
345 *phys. Res. Lett.* 2, 409–412.
- 346 Gubbins, D., 1987. Mechanism for geomagnetic polarity reversals. *Nature* 326, 167–169.
- 347 Gubbins, D., Bloxham, J., 1985. Geomagnetic field analysis - III. Magnetic fields on the  
348 core-mantle boundary. *Geophys. J. R. Astron. Soc.* 80, 695–713.
- 349 Holme, R., 2000. Electromagnetic core-mantle coupling III: laterally varying mantle con-  
350 ductance. *Phys. Earth Planet. Int.* 117, 329–344.
- 351 Jackson, A., 2003. Intense equatorial flux spots on the surface of the Earth's core. *Nature*  
352 424, 760–763.
- 353 Jackson, A., Jonkers, A. R. T., Walker, M. R., 2000. Four centuries of geomagnetic secular  
354 variation from historical records. *Phil. Trans. R. Soc. Lond. A* 358, 957–990.

- 355 Johnson, C. L., Constable, C. G., 1995. The time-averaged geomagnetic field as recorded  
356 by lava flows over the past 5 Myr. *Geophys. J. Int.* 122, 489–519.
- 357 Johnson, C. L., Constable, C. G., 1997. The time-averaged geomagnetic field: global and  
358 regional biases for 0-5 Ma. *Geophys. J. Int.* 131, 643–666.
- 359 Jonkers, A. R. T., Jackson, A., Murray, A., 2003. Four centuries of geomagnetic data from  
360 historical records. *Rev. Geophys.* 41,2, doi:10.1029/2002RG000115.
- 361 Kelly, P., Gubbins, D., 1997. The geomagnetic field over the past 5 Myr. *Geophys. J. Int.*  
362 128, 315–330.
- 363 Korte, M., Constable, C. G., 2005. Continuous geomagnetic field models for  
364 the past 7 millennia: 2. CALS7K. *Geochem., Geophys., Geosys.* 6, Q02H16,  
365 doi:10.1029/2004GC000801.
- 366 Korte, M., Constable, C. G., 2008. Spatial and temporal resolution of millennial scale  
367 geomagnetic field models. *J. Adv. Space Res.* 41, 57–69.
- 368 Korte, M., Donadini, F., Constable, C., 2009. Geomagnetic field for 0-3ka: 2. a  
369 new series of time-varying global models. *Geochem. Geophys. Geosys.* 10, Q06008,  
370 doi:10.1029/2008GC002297.
- 371 Korte, M., Genevey, A., Constable, C. G., Frank, U., Schnepf, E., 2005. Continuous  
372 geomagnetic field models for the past 7 millennia: 1. a new global data compilation.  
373 *Geochem., Geophys., Geosys.* 6, Q02H15, doi:10.1029/2004GC000800.
- 374 Lesur, V., Wardinski, I., Rother, M., Manda, M., 2008. GRIMM: the GFZ Reference  
375 Internal Magnetic Model based on vector satellite and observatory data. *Geophys. J.*  
376 *Int.* 173, 382–394.
- 377 Macmillan, S., Maus, S., 2005. Modelling the Earth's magnetic field; the 10th generation  
378 IGRF. *Earth, Planets, Space* 57(12), 1135–1140.

- 379 McElhinny, M. W., Senanayake, W. E., 1982. Variations in the geomagnetic dipole: I. The  
380 past 50 000 years. *J. Geomag. Geoelectr.* 34, 39–51.
- 381 Mothersill, J. S., 1996. Paleomagnetic results from lakes Victoria and Albert, Uganda.  
382 *Studia geoph. et geod.* 40, 25–35.
- 383 Olsen, N., Mande, M., Sabaka, T. J., Toffner-Clausen, L., 2009. CHAOS-2 – a geomag-  
384 netic field model derived from one decade of continuous satellite data. *Geophys. J. Int.*  
385 179, 1477–1487.
- 386 Willis, A. P., Sreenivasan, B., Gubbins, D., 2007. Thermal core-mantle interaction: Ex-  
387 ploring regimes for ‘locked’ dynamo action. *Phys. Earth Planet. Int.* 165, 83–92.
- 388 Yang, S., Odah, H., Shaw, J., 2000. Variations in the geomagnetic dipole moment over the  
389 last 12000 years. *Geophys. J. Int.* 140, 158–162.